Interannual and Seasonal Variability of Snow Depth Scaling Behavior in a Subalpine Catchment

6 authors, including:

Pablo A. Mendoza
University of Chile
30 PUBLICATIONS   406 CITATIONS

SEE PROFILE

Keith N. Musselman
University of Colorado Boulder
42 PUBLICATIONS   1,095 CITATIONS

SEE PROFILE

James Mcphee
University of Chile
107 PUBLICATIONS   1,928 CITATIONS

SEE PROFILE

Some of the authors of this publication are also working on these related projects:

Project   Postdoctoral fellow, Center for Climate and Resilience Research (CR2) <www.cr2.cl> View project

Project   Climate-Adaptation-Santiago View project

Interannual and Seasonal Variability of Snow Depth Scaling Behavior in a Subalpine Catchment

Pablo A. Mendoza[1,2] (iD), **Keith N. Musselman[3]** (iD), **Jesús Revuelto[4]** (iD), **Jeffrey S. Deems[5]** (iD), **J. Ignacio López-Moreno[4]** (iD), **and James McPhee[1,2]** (iD)

[1]Department of Civil Engineering, Universidad de Chile, Santiago, Chile, [2]Advanced Mining Technology Center, Universidad de Chile, Santiago, Chile, [3]Institute of Arctic and Alpine Research, University of Colorado, Boulder, CO, USA, [4]Pyrenean Institute of Ecology, CSIC, Zaragoza, Spain, [5]National Snow and Ice Data Center, University of Colorado, Boulder, CO, USA

Abstract Understanding and characterizing the spatial distribution of snow are critical to represent the energy balance and runoff production in mountain environments. In this study, we investigate the interannual and seasonal variability in snow depth scaling behavior at the Izas experimental catchment of the Spanish Pyrenees (2,000 to 2,300 m above sea level). We conduct variogram analyses of 24 snow depth maps derived from terrestrial light detection and ranging scans, acquired during six consecutive snow seasons (2011–2017) that span a range of hydroclimatic conditions. We complement our analyses with bare ground topography data and wind speed and direction measurements. Our results show temporal consistency in the spatial variability of snow depth, with short-range fractal behavior and scale break lengths that are similar to the optimal search distance (25 m) previously reported for the topographic position index, a terrain-based predictor of snow depth. Beyond the 25-m scale break, there is little to no fractal structure. We report a long-range scale break of the order of 185–300 m for most dates—aligned with the dominant wind direction—and patterns between anisotropies in scale break lengths of shallow snow cover and directional terrain scaling behavior. The temporal consistency of snow depth scaling patterns suggests that, in addition to guiding the spatial configuration of physically based models, fractal analysis could be used to inform the design of independent variables for statistical models used to predict snow depth and its variability.

1. Introduction

Mountainous regions are an essential source of freshwater around the world, with many playing a primary role for downstream areas (Viviroli et al., 2007). In these environments, snow is a major component of the hydrologic cycle since its presence/absence has large effects on the surface energy and water balances (Andreadis et al., 2009). Moreover, the spatial variability of snow accumulation influences the magnitude, timing and persistence of snow melt (Clark et al., 2011; Freudiger et al., 2017), and the timing of snow disappearance. Hence, understanding and characterizing snow depth variability across a hierarchy of scale lengths are crucial for the design of accurate measurement and modeling systems, especially considering the need to quantify water resources under changing climatic conditions (e.g., Barnett et al., 2005; Mankin et al., 2015; Viviroli et al., 2011).

Over recent decades, fractal analysis has arisen as a powerful technique to depict the spatial and temporal variability of geophysical variables (e.g., Mark & Aronson, 1984; Skøien et al., 2003). Notably, water resources science and engineering was among the first areas where the fractal concept was applied to solve actual problems, with early applications in operational hydrology (e.g., Hurst, 1951; Mandelbrot & Wallis, 1968). Mandelbrot (1977, 1982) coined the term "fractal" and used computer-based images to illustrate the notion of "a structure that has infinite detail" (Deems et al., 2006) within a range of spatial scales. More generally, a fractal can be understood as an object whose subsets preserve the geometric or statistical characteristics of the whole under transformations of scales (Mandelbrot, 1982)—a property referred to as scale invariance or self-similarity. Additionally, the term has been typically reserved for highly irregular objects with detailed structures that cannot simply be described with traditional Euclidean geometry (Sun et al., 2006). The literature is quite rich in applications of fractal concepts to characterize patterns in hydrology, including rainfall (Olsson et al., 1993), river network structures (Tarboton et al., 1988), floods (Alipour

et al., 2016), stream chemistry (Kirchner et al., 2000), soil moisture (Korres et al., 2015), and subsurface processes (Molz et al., 2004).

In particular, the fractal concept has been exploited to understand and characterize the scaling behavior of snow and other variables affecting its distribution. Initial efforts using manual measurements reported self-similar behavior in snow depth and snow water equivalent (SWE) before a "cutoff length" on the order of tens of meters (e.g., Arnold & Rees, 2003; Kuchment & Gelfan, 2001; Shook & Gray, 1996). This cutoff term—also referred to as scale break length, scale break distance, or simply scale break—is typically assumed to infer a change in the physical processes driving the spatial structure of the snow. Because manual snow measurements are time consuming and potentially risky, the emergence of light detection and ranging (lidar) technology has become a milestone for snow measurement (e.g., Deems et al., 2013) and scaling studies (e.g., Fassnacht & Deems, 2006; Lehning et al., 2011; Tedesche et al., 2017).

Although water resource scientists, engineers, and managers ultimately need SWE for hydrological predictions in mountain environments (e.g., Mendoza et al., 2014; Perkins et al., 2009; Rosenberg et al., 2011), characterizing the spatial variability of snow depth is still critical to properly quantify SWE variability since the former is considerably larger than the spatial variability of snow density (López-Moreno, Fassnacht, et al., 2013). To this end, the joint use of lidar technology, meteorological observations, and fractal concepts has paved the way to improve understanding of snow depth patterns. For example, Deems et al. (2006) and Trujillo et al. (2007) used variograms and power spectra, respectively, to contrast fractal parameters in snow depth, topography, and vegetation derived from lidar data. Using the same airborne laser scanning (ALS) data sets acquired near the maximum snow accumulation date, both studies found two scaling ranges with distinct fractal patterns in snow depth separated by consistent scale breaks, suggesting that these could inform the choice of spatial scales in snow models. Unlike Trujillo et al. (2007), Deems et al. (2006) found scale breaks in the sum of surface elevation and vegetation height, with values of the same order of magnitude as snow. Later, Trujillo et al. (2009) found substantial differences in the snow scaling behavior of two areas with similar topography but different vegetation and wind influences (i.e., forest vs. tundra). Mott et al. (2011) compared the scaling behavior of snow depth measurements with modeled high-resolution wind fields and snow depth changes, concluding that wind velocity distributions have similar anisotropies to those of snow depth. Scipión et al. (2013) examined potential links between snow accumulation and snowfall through variogram analysis in the Swiss Alps, finding smoother spatial patterns of radar-measured snowfall compared to ALS snow depth measurements, pointing to the dominant role of wind redistribution. He et al. (2019) used lidar data to analyze the geostatistical structure of 1×1-km grids with differing topographies and land cover characteristics, finding correlation lengths smaller than 100 m in most sites and increasing fractal dimensions with greater forest cover.

Despite the above progress, only a few studies have investigated the temporal "consistency" (Clemenzi et al., 2018; Deems et al., 2008) or "persistence" (Helfricht et al., 2014; Schirmer & Lehning, 2011) in the spatial structure of snow. Deems et al. (2008) analyzed snow depth maps obtained for two sites near two maximum accumulation dates, reporting very similar short- and long-range fractal dimensions, similar anisotropies, and comparable scale breaks across years. Schirmer and Lehning (2011) explored intra-annual variations in snow scaling behavior on three topographically distinct slopes within an alpine domain without vegetation. They found different snow depth structures at these sites and consistent fractal behavior at the end of two accumulation seasons. Helfricht et al. (2014) examined the fractal behavior of snow depth at the time of maximum accumulation in a partially glacierized catchment (36 km^2) using data from five ALS surveys—conducted over five nonconsecutive years. They obtained scale breaks within the range 18–22 m and short- (long-) range fractal dimensions of 2.34–2.66 (2.91–2.93). More recently, Clemenzi et al. (2018) investigated snow depth patterns on a glacier and seven subdomains at the end of two snow accumulation seasons (2007 and 2011), finding scale breaks in the range 10–35 m, consistent with fractal parameters across years, and identifying wind as a key control for directionality and anisotropy. Although the above investigations have demonstrated temporal consistency in fractal parameters at various sites over multiple time periods, no long-term study has explored snow fractal patterns over a span of consecutive years.

In this paper, we investigate the temporal variability of snow depth scaling behavior in a subalpine, unforested catchment, using a rich data set consisting of 24 terrestrial laser scanner (TLS, lidar technology)

surveys acquired over six consecutive snow seasons (Revuelto et al., 2017a). The database provides unique opportunities to: (i) compare the fractal behavior of snow depth between maximum accumulation and melt across snow seasons, (ii) assess the temporal consistency of snow structure through individual snow seasons, and (iii) identify the main controls on fractal parameters.

2. Material and Methods

2.1. Study Domain

Our study site is the Izas experimental catchment (Figure 1a; 42°44′N, 0°25′W) in the Spanish Pyrenees. The Pyrenees lie on the northwestern Iberian Peninsula—between the Atlantic and the Mediterranean Sea—and can be classified as a temperate or midlatitude mountain range. The 55-ha catchment has an elevation range between 2,000 and 2,300 m above sea level. There are no trees in this domain, and the basin is mostly subalpine grassland with rocky outcrops in the steeper areas (less than 15% of the study area). The catchment is predominantly east facing, with some northern and southern aspects. The topography includes flat, concave and convex areas. The mean slope of the catchment is 16° (López-Moreno, Pomeroy, et al., 2013).

The mean annual precipitation in the catchment is 2,000 mm, of which snowfall accounts for approximately 50% (Anderton et al., 2004). The mean annual air temperature is 3°C, and the mean daily temperature is <0°C for an average of 130 days each year. Snow covers much of the catchment area from November to the end of May (López-Moreno et al., 2017).

2.2. Data

We use one bare ground digital elevation model (DEM) and 24 snow depth distribution maps derived from TLS surveys conducted during the period 2011–2017 (Table 1). These data sets are fully described in Revuelto, López-Moreno, Azorin-Molina, Zabalza et al., 2014; Revuelto 2017a) and only briefly reviewed here. The maps were obtained by processing point cloud data sets of snow and snow-free surface heights acquired with a long-range TLS device (RIEGL LPM-321; Figure 1b) from two scanning positions (Figure 1c) selected to minimize shading effects. To ensure a consistent comparison of scans made on different survey days, 12 reflective targets (Figure 1b) were placed as coordinate reference points. The point clouds were postprocessed to obtain 1-m horizontal resolution elevation grids with and without snow, which were used to derive snow depth distribution maps with a mean absolute snow depth error of 0.07 m (Revuelto, López-Moreno, Azorin-Molina, Zabalz et al., 2014). The resulting snow depth maps are diverse in terms of domain statistics (e.g., mean, maximum value, and coefficient of variation) and snow-covered area (see Table 1 for details).

Based on the high interannual variability of snow depth (see supporting information, Figure S1), we group our snow seasons between high (2012/2013, 2013/2014, and 2015/2016) and low (2011/2012, 2014/2015, and 2016/2017) snow depth magnitude and also group scans by accumulation and melt for subsequent analyses on scaling behavior.

We complement our analyses with wind speed and direction data collected by an anemometer (Young alpine model) located at a meteorological station (see location in Figure 1c), 8 m above the ground. The Pyrenees are typically affected by strong westerly to northerly winds (López-Moreno, Pomeroy, et al., 2013; Revuelto, López-Moreno, Azorin-Molina, & Vicente-Serrano, 2014; Revuelto et al., 2017a), with the exception of southerly winds during the snowmelt period. We illustrate this in Figure 2, where wind roses are displayed for all snow seasons for times when (i) wind speeds exceeded 4 m s^{-1}, following Li and Pomeroy (1997)—who reported that threshold for blowing snow occurrence in dry snow—and (ii) air temperature was below 0°C when snow transport by wind is most likely to occur (Trujillo et al., 2007). Similar frequency distributions are obtained when including all air temperatures or setting the wind speed threshold at 5 m s^{-1} (Clemenzi et al., 2018; Deems et al., 2008; not shown here).

2.3. Variogram Analysis

The variogram is a function to examine the degree of spatial dependency in a random field. The variogram can be particularly useful to quantify spatial patterns in fractional Brownian surfaces—i.e., those that exhibit
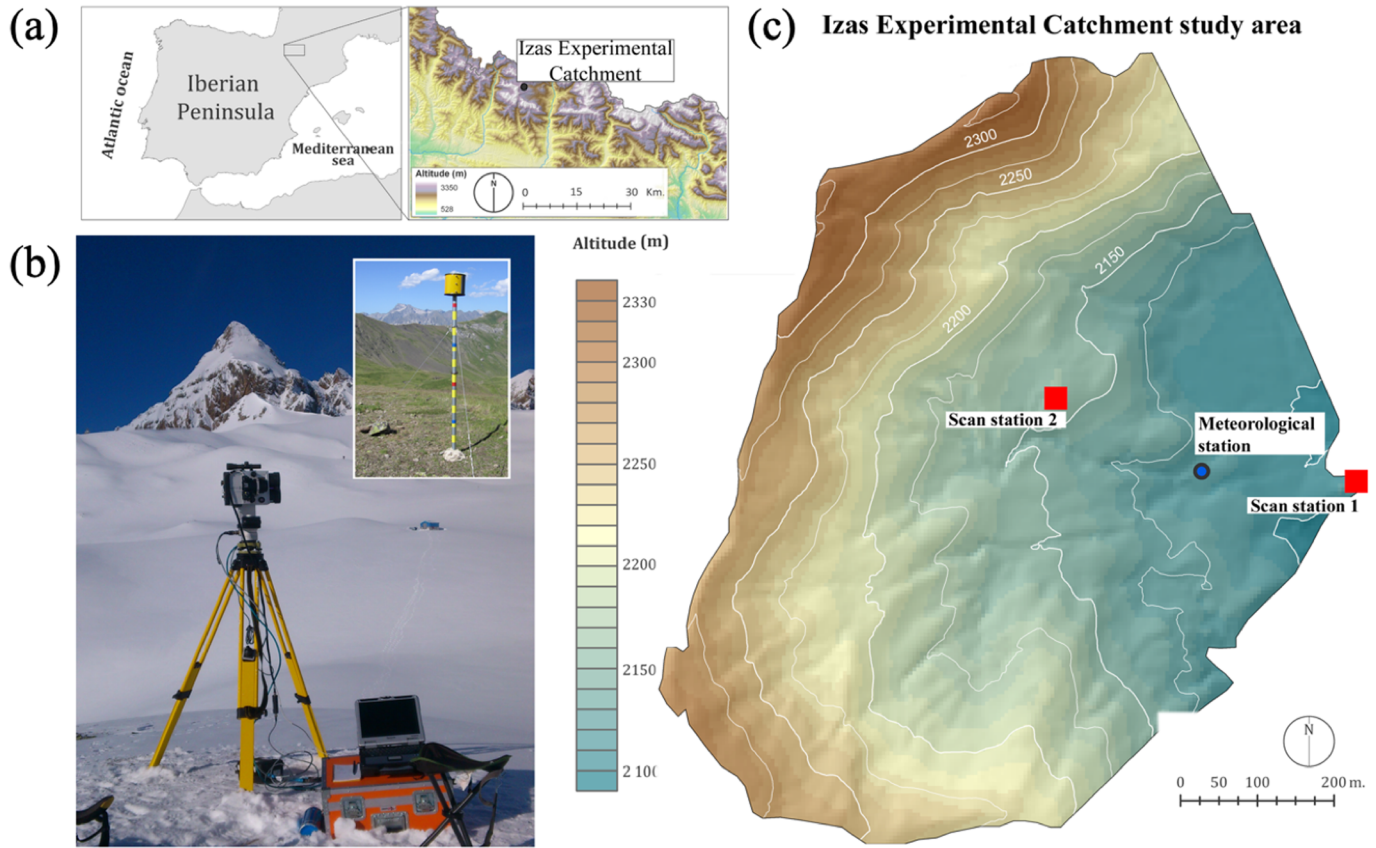
Figure 1. (a) Location of the Izas experimental catchment. (b) RIEGL LPM-321 TLS mounted on the tripod during an acquisition campaign; the upper-right part shows one of the 12 fixed reflective targets fixed on the terrain. (c) Relative location of the scanning points and meteorological stations.

fractal, self-similar, or scale-free behavior (Mark & Aronson, 1984). Further, it can be used as a diagnostics tool for objects whose scaling behavior is unknown (Sun et al., 2006).

Given a distance h, the semivariance can be computed as

$$\widehat{\gamma}(h) = \frac{1}{2|N(h)|} \sum_{(i,j)\,\in\,N(h)} \left(z_j - z_i\right)^2,\tag{1}$$

where z_i and z_j are snow depth values for points separated by a lag distance h and $N(h)$ is the number of data points at a given distance h (Oliver & Webster, 2007). If snow depth shows self-similar (i.e., fractal) behavior within a range of h, it should be possible to fit a power law with the form (Deems et al., 2006)

$$\gamma(h) = \alpha h^\beta.\tag{2}$$

The exponent β can be subsequently used to compute the fractal dimension, using the formula proposed by Mark and Aronson (1984):

$$D = 3 - \frac{\beta}{2}.\tag{3}$$

The fractal dimension D is typically interpreted as "a measure of an object's ability to 'fill' the space in which it resides" (Sun et al., 2006)—that is, as the object of interest becomes more irregular, it fills more space and a larger fractal dimension is expected. Although fractal dimensions are consistent with the spatial dimensions of Euclidean geometry, they can also take noninteger values. Hence, curves are characterized by fractal dimensions between 1 and 2, while surfaces have associated D values between 2 and 3. For

Table 1

Domain-averaged mean (mean SD) and maximum (max SD) snow depth values, coefficient of variation (CV), snow-covered area (SCA), and omnidirectional fractal parameters (D_S, L_1, and L_2) for the observed TLS snow depth distributions. For the short-range fractal dimension, 95% confidence intervals are displayed in parenthesis

Snow season	Date	Mean SD (m)	Max SD (m)	CV	SCA %	Short range R^2	D_S	L_1 (m)	L_2 (m)
2011/2012	22 Feb	0.48	6.46	1.34	67.2	0.99	2.39 (2.37–2.41)	18.0	365.2
	2 Apr	0.20	4.14	2.12	33.5	0.99	2.51 (2.49–2.53)	17.9	304.3
	17 Apr	0.54	5.45	1.10	94.1	0.99	2.46 (2.44–2.48)	17.4	301.2
	2 May	*0.93*	*8.64*	*0.73*	*98.8*	*0.99*	*2.43 (2.41–2.45)*	*17.7*	*305.6*
	14 May	**0.23**	**4.76**	**2.18**	**30.9**	**0.99**	**2.45 (2.43–2.47)**	**18.1**	**285.8**
2012/2013	17 Feb	3.03	11.28	0.61	98.8	1.00	2.26 (2.25–2.27)	20.6	-
	3 Apr	*3.25*	*12.03*	*0.56*	*100.0*	*1.00*	*2.25 (2.24–2.26)*	*20.1*	-
	25 Apr	2.47	10.69	0.69	96.3	1.00	2.25 (2.24–2.26)	20.0	-
	6 Jun	1.96	10.02	0.86	86.4	0.99	2.39 (2.37–2.42)	24.3	-
	12 Jun	1.63	9.42	0.96	77.1	1.00	2.24 (2.23–2.25)	19.1	-
	20 Jun	**1.11**	**8.38**	**1.19**	**67.0**	**1.00**	**2.28 (2.27–2.29)**	**18.7**	-
2013/2014	3 Feb	2.20	10.03	0.60	96.0	1.00	2.3 (2.29–2.32)	19.1	-
	22 Feb	2.58	11.15	0.58	98.6	1.00	2.29 (2.28–2.3)	20.0	-
	9 Apr	*2.58*	*11.18*	*0.65*	*89.0*	*1.00*	*2.26 (2.25–2.27)*	*20.1*	-
	5 May	**1.67**	**9.71**	**0.87**	**75.2**	**1.00**	**2.27 (2.26–2.29)**	**19.7**	-
2014/2015	6 Nov	0.19	11.77	0.96	85.0	1.00	2.85 (2.84–2.85)	12.2	-
	26 Jan	0.66	4.88	0.96	89.3	0.99	2.45 (2.43–2.46)	18.1	394.5
	6 Mar	*2.02*	*11.55*	*0.76*	*94.0*	*1.00*	*2.28 (2.27–2.3)*	*19.8*	-
	12 May	**0.38**	**7.76**	**1.85**	**56.0**	**1.00**	**2.39 (2.37–2.4)**	**20.3**	**385.3**
2015/2016	4 Feb	0.98	8.65	0.74	91.1	0.99	2.49 (2.47–2.5)	18.0	228.9
	25 Apr	***2.25***	***9.28***	***0.52***	***97.0***	***1.00***	***2.32 (2.31–2.33)***	***18.4***	-
	26 May	0.80	8.48	1.36	74.8	0.99	2.8 (2.79–2.81)	37.8	282.3
2016/2017	***20 Jan***	***1.20***	***6.34***	***0.63***	***93.0***	***1.00***	***2.43 (2.42–2.45)***	***18.6***	***306.0***
	8 May	**0.56**	**6.94**	**1.38**	**57.2**	**0.99**	**2.38 (2.36–2.4)**	**19.0**	**299.0**

Maximum accumulation scans
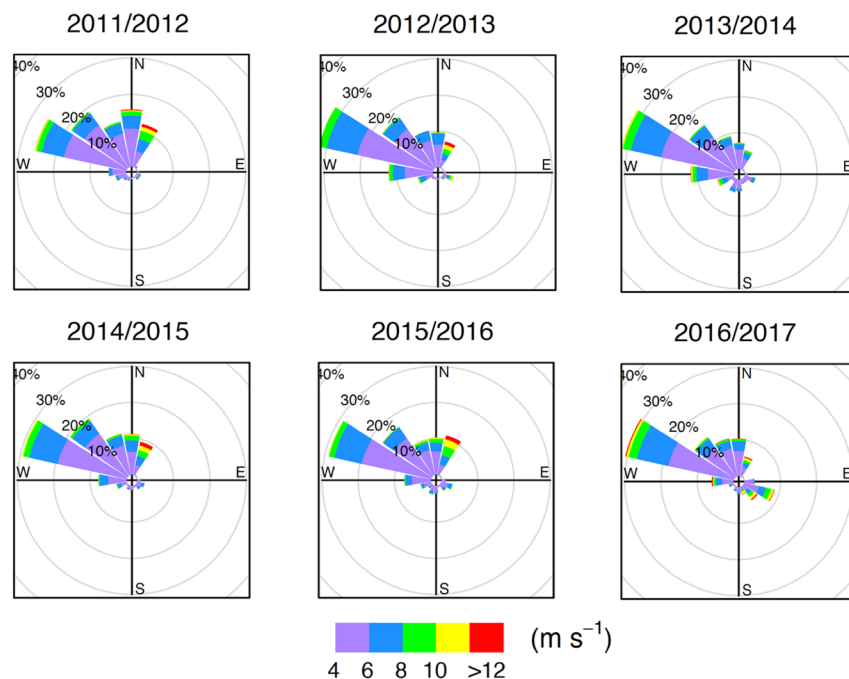**Last *melt* season *scans***

Figure 2. Wind direction frequency distributions for the period November–June and all snow seasons, considering only wind speeds >4 m s^{-1} and air temperature below 0°C.

the specific case of snowpack, the fractal dimension D can be used to describe the level of irregularity (Schirmer & Lehning, 2011), with $D \sim 2$ indicating a nearly planar Euclidean surface and values close to 3 reflecting more complex or "rougher" behavior.

In this study, we define 46 bins to compute omnidirectional variograms, which include all point pairs regardless of their direction; and directional variograms, which include only point pairs within a specified direction. We use a maximum distance of 750 m—approximately the diameter of the largest circle that can be fit inside the study domain (following Deems et al., 2006, 2008)—and 16 angular classes of 22.5° for directional variograms. To assess the possibility of different scaling regimes in snow depth patterns, and test whether fractal behavior exists in those distance ranges, we perform the following checks:

1. Conduct a change point analysis on variograms in the log-log space to find clusters of points sharing a similar trend. We use the E-divisive nonparametric technique (Matteson & James, 2014), which combines bisection and a divergence measure for multivariate distributions. The change point detection is performed using the "ecp" package (James & Matteson, 2014), implemented in the statistical software "R" (http://www.r-s/).
2. Fit linear least squares regression models for variogram points from each group in log-log space (i.e., power laws in raw space) and set intercept estimates as candidate scale break points.
3. Verify whether the changes in the slopes of log-log linear models are larger than 20% and that 95% confidence limits of the regression slopes do not overlap. If these conditions are satisfied, we conduct a visual inspection of variograms to confirm that the scale break exists and, hence, that there is more than one scaling region.
4. Check whether the linear models adjusted in step (2) show R^2 greater than 0.9. If this is the case, scaling behavior is described as fractal (Deems et al., 2006, 2008) and the associated fractal dimension is computed with Equation 3.

The above analyses were first conducted for omnidirectional and second for directional variograms to detect and characterize potential anisotropies in snow depth scaling patterns. It should be noted that this approach recognizes that a surface could be fractal within some range of lag distances and show no spatial correlation in others, a behavior that has been reported in the past for snow depth (e.g., Shook & Gray, 1996).

We illustrate the variogram analysis approach in Figure S2, which also compares the quality of fit of the log-log linear model used to assess whether scale breaks and fractals exist, with three alternative geostatistical models—exponential, Gaussian, and spherical—adjusted for the entire range of points. The results show that the multisegment log-log linear models provide lower root mean squared errors (RMSE), lower biases, and higher correlations against observations since the alternative models fail to capture the scaling behavior beyond the second scale break distance. Although further model intercomparisons were conducted for the various scaling ranges identified here (not shown), the remainder analyses and discussions are limited to linear law types in log-log space since our end goal is to assess whether fractal behavior exists and also if such structure persists in time.

2.4. Potential Controls on Fractal Parameters

We explore possible factors explaining the snow depth scaling behavior and detected anisotropies, as well as the temporal variability in snow depth fractal parameters. First, we compute omnidirectional and directional variograms for the bare-earth topography to compare fractal characteristics and potential similarities with snow depth.

We conduct a two-sample t test on the short-range fractal dimensions and scale break lengths obtained from omnidirectional and directional (perpendicular and parallel to prevailing winds) variograms. The samples are generated from splitting fractal parameter values by (i) accumulation (13) vs. melt (11) lidar scans and (ii) type of season (11 low-snow vs. 13 high-snow seasons). If the p values are larger than the level of significance ($\alpha = 0.05$), we accept the null hypothesis that the means of the two samples are the same, but do not consider the probability of making a Type II error. Further, we perform a correlation analysis between omnidirectional and directional fractal parameters against basin-wide snow descriptors (mean snow depth, coefficient of variation, and snow-covered area) for the domain. We report Spearman rank correlation coefficients and associated p values to assess whether these are statistically significant at the 95% confidence level.
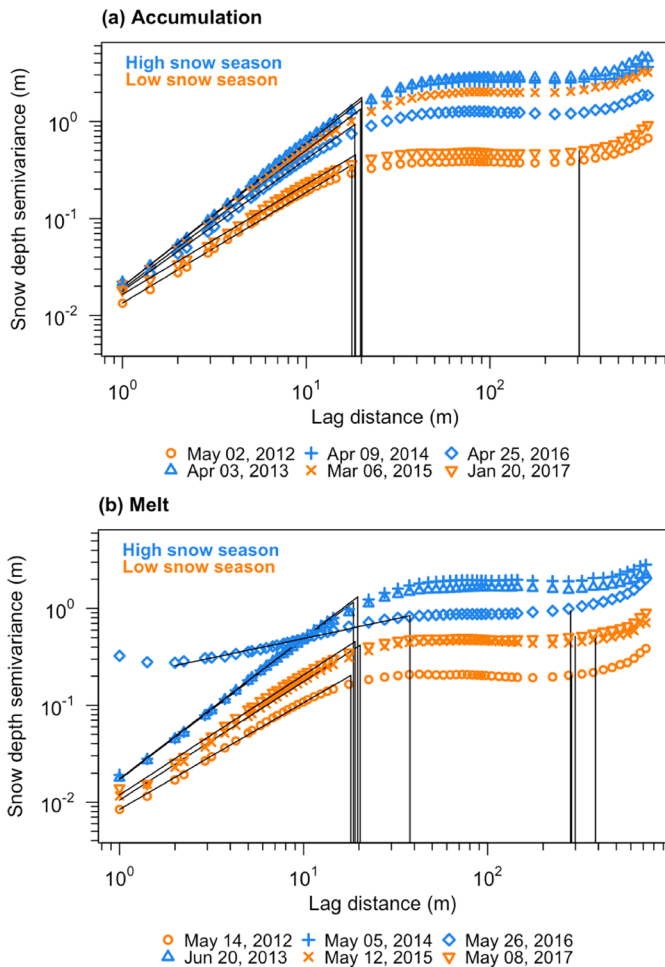
Figure 3. Omnidirectional variograms for snow depth from (a) maximum snow accumulation and (b) last melt season scans in snow seasons 2011/2012 to 2016/2017. Vertical lines represent scale break lengths, and diagonal lines represent log-log linear models with $R^2 > 0.9$.

3. Results

3.1. Interannual Variability

We first compare scaling patterns among lidar scan dates that captured maximum accumulation and melt periods from six snow seasons. We select from each snow season (i) the map with the largest spatial average snow depth and (ii) the last measurement date from the melt season. Figure 3 displays omnidirectional variograms from (a) accumulation and (b) melt season snow depth data sets. All accumulation season variograms (Figure 3a) show clear scale breaks within the range 17.7–20.1 m (see Table 1 for details), with fractal behavior up to those breaks. Similar scale breaks (Mott et al., 2011) and—more importantly—interannual consistency have been previously reported in studies of ice-free domains (Deems et al., 2008; Helfricht et al., 2014; Schirmer & Lehning, 2011) and glacierized sites (Clemenzi et al., 2018). Our results differ in that there is no evidence of fractal behavior beyond those scale breaks, after which a nearly flat shape arises up to ~300 m. A second omnidirectional scale break is only detected for a single scan on 20 January 2017 since the other data sets do not show a statistically significant difference in semivariance slopes beyond the first break. Short-range fractal dimensions span a range of 2.3–2.4, which is close to values reported in other unvegetated domains (e.g., Helfricht et al., 2014; Schirmer & Lehning, 2011).

Figure 3b compares omnidirectional variograms for the last melt scan from each season. These data sets also show strong spatial correlation up to a short-range scale break, with fractal parameter values of the same order of magnitude as those found for maximum accumulation—that is, D_S ~ 2.2–2.5 and L_1 ~ 18–20.3 m (Table 1)—with the exception of the scan conducted on 26 May 2016, for which D_S ~ 2.8 and L_1 ~ 37.8 m, respectively. Four out of six snow depth distributions also exhibit a secondary scale break length spanning 282–385 m.

We also examine possible anisotropies in snow depth scaling behavior by computing fractal parameters from directional variograms—specifically the short-range fractal dimension D_S, the primary scale break (L_1), and the secondary scale break (L_2) (Figure 4). During maximum snow accumulation days (Figure 4a), no evident anisotropies are found for D_S. Nevertheless, the largest L_1 values are mostly aligned along the W-E direction, while SW-NE (i.e., perpendicular to prevailing winds) anisotropies are observed for L_2. Moreover, no clear distinction in the shape of anisotropies is found between high- vs. low-snow seasons.

The lack of anisotropies in D_S is also observed for the end-of-snowmelt scans (Figure 4b). Nevertheless, the largest L_1 values are perpendicular to dominant winds (NW-SE). Both the magnitude and anisotropies in D_S and L_1 were consistent in low-snow seasons. When analyzing secondary scale breaks, we find that the largest values of L_2 align with the N-S direction, except 26 May 2016 and 8 May 2017 for which SW-NE anisotropies are observed.

3.2. Seasonal Variability

Table 1 summarizes fractal dimensions and scale break lengths from omnidirectional variograms computed for all lidar data sets (Figure 5), showing small intra-annual variations in D_S and short-range scale break lengths (L_1) except in snow seasons 2014/2015 and 2016/2017, which are biased by relatively shallow snowpack measured on 6 November 2014 (accumulation) and 26 May 2016 (melt). If one excludes those data sets, we obtain D_S and L_1 values spanning 2.3–2.5 and 17–24 m, respectively. Omnidirectional secondary scale breaks lengths are only detected on 11 days, and their values range between 200–400 m.
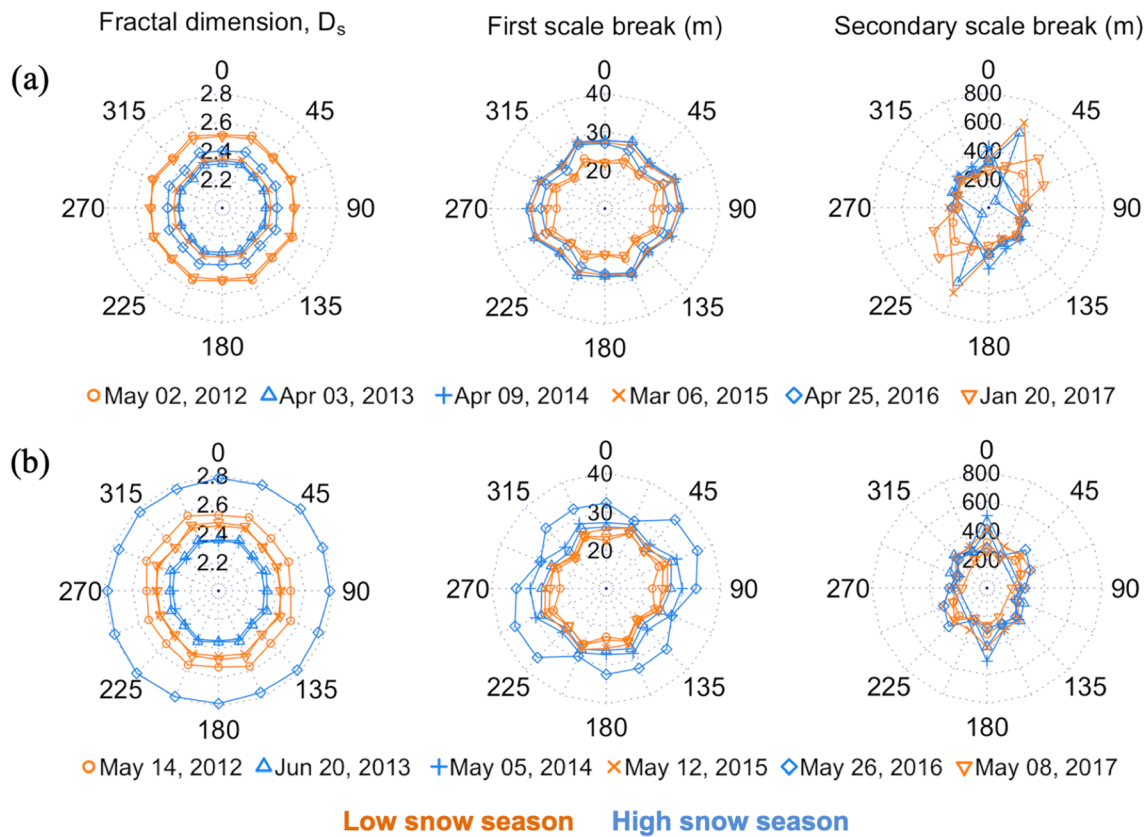
Figure 4. Snow depth fractal parameters by azimuth, obtained for (a) maximum snow accumulation lidar scans and (b) last melt season scans.

Further, the comparison of omnidirectional variograms (Figure 5) from the same snow season reveals little variation in curve shapes and well-defined scale break lengths, except for the scans obtained on 6 November 2014 and 26 May 2016. For data sets acquired during snow seasons 2011/2012 and 2012/2013, scale break lengths span 17–18 and 19–24 m, respectively, which are similar to the optimal search distance of 25 m found by Revuelto, López-Moreno, Azorin-Molina, & Vicente-Serrano, et al. (2014) for the topographic position index (TPI), a predictor of snow depth that is related to the shape and length scale of terrain undulations susceptible to snow scour and wind deposition. Moreover, the existence of more than one distance range with snow depth fractal behavior is only detected for two scans across the domain (Figures 5d and 5e), unlike past studies reporting two different scaling patterns near maximum accumulation (e.g., Clemenzi et al., 2018; Deems et al., 2006; Schirmer & Lehning, 2011). Such behavior has been described as "multifractal" by some authors (Deems et al., 2006; Schirmer & Lehning, 2011), although—broadly speaking—the concept is typically considered to involve a continuous spectrum of fractal dimensions (Mandelbrot, 1988).

Figure 6 displays—for each snow season—radar plots with fractal dimensions and scale breaks computed from directional variograms. In general, directional variations in D_S are almost negligible, departing from previous studies such as Deems et al. (2006) and Schirmer and Lehning (2011), who found the largest D_S values perpendicular to dominant winds, and Clemenzi et al. (2018), who reported larger D_S values aligned with prevailing winds. This result could stem from the difficulty of characterizing a basin-representative wind field using observations from a single station, pointing also to additional process interactions at this site. Figure 6 also shows some important variations in scale break anisotropies from the accumulation period (green lines) to the melt season (red lines)—for example, L_1 during 2014/2015 and 2015/2016 and L_2 in all seasons.

Figure 7 illustrates the temporal development of fractal parameters from omnidirectional and directional (22.5° and 112.5°) variograms across all scan dates. We plot these two directions to examine possible connections with prevailing winds and compare our results with previous studies. Although dominant wind
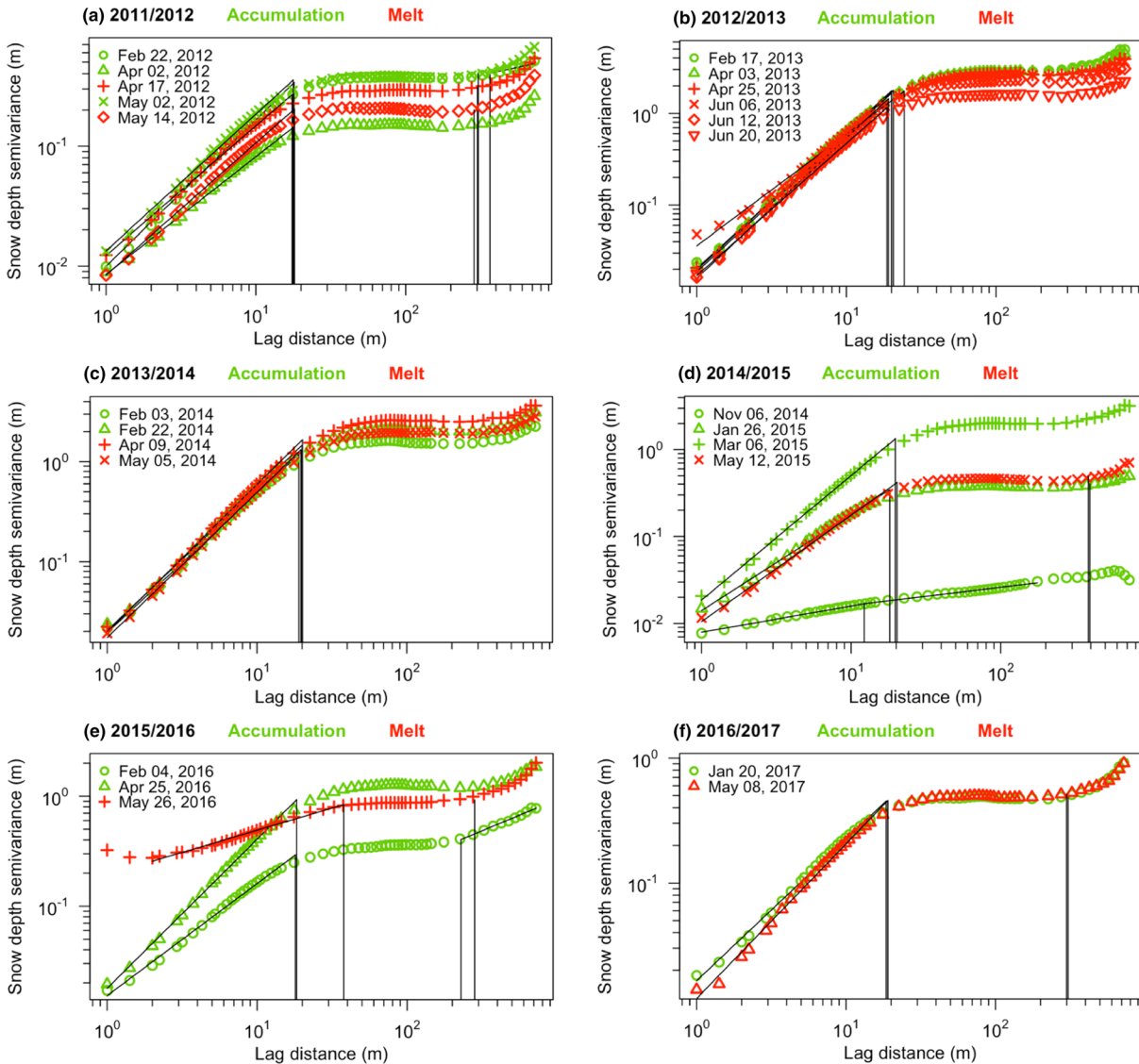
Figure 5. Omnidirectional variograms for all snow depth maps grouped by snow season. Vertical lines represent scale break lengths, and diagonal lines represent log-log linear models with $R^2 > 0.9$.

directions at the Izas experimental catchment span 270°–315°, we choose the direction associated with the largest frequency obtained in Figure 2 (112.5°, equivalent to 292.5°). Overall, smaller short-range fractal dimensions are obtained for the seasons with the largest snow accumulations (i.e., 2012/2013 and 2013/2014; Figure 7a). Moreover, directional D_S values are larger than omnidirectional D_S in most cases, and fractal behavior beyond the primary scale break (i.e., filled or thin open symbols) is rarely detected. Figure 7b shows that—except for the scan acquired on 26 May 2016—directional L_1 values are larger than omnidirectional L_1, and there are not consistently larger L_1 values along 22.5° compared to those derived from 112.5°, as found by Schirmer and Lehning (2011). However, we find larger L_1 values at the end of the 2014/2015 and 2015/2016 winters and changes in the shape of scale break anisotropies throughout these seasons.

Interestingly, Figure 7c reveals a temporally consistent secondary scale break L_2 of the order of hundreds of meters, aligned with prevailing winds. Further, L_2 values perpendicular to dominant winds are, in most cases, larger than those from 112.5° variograms. To our knowledge, no studies have reported the existence of this long-range scale break and, even more, its interannual and intra-annual consistencies. The practical implications of this finding are discussed in section 4.
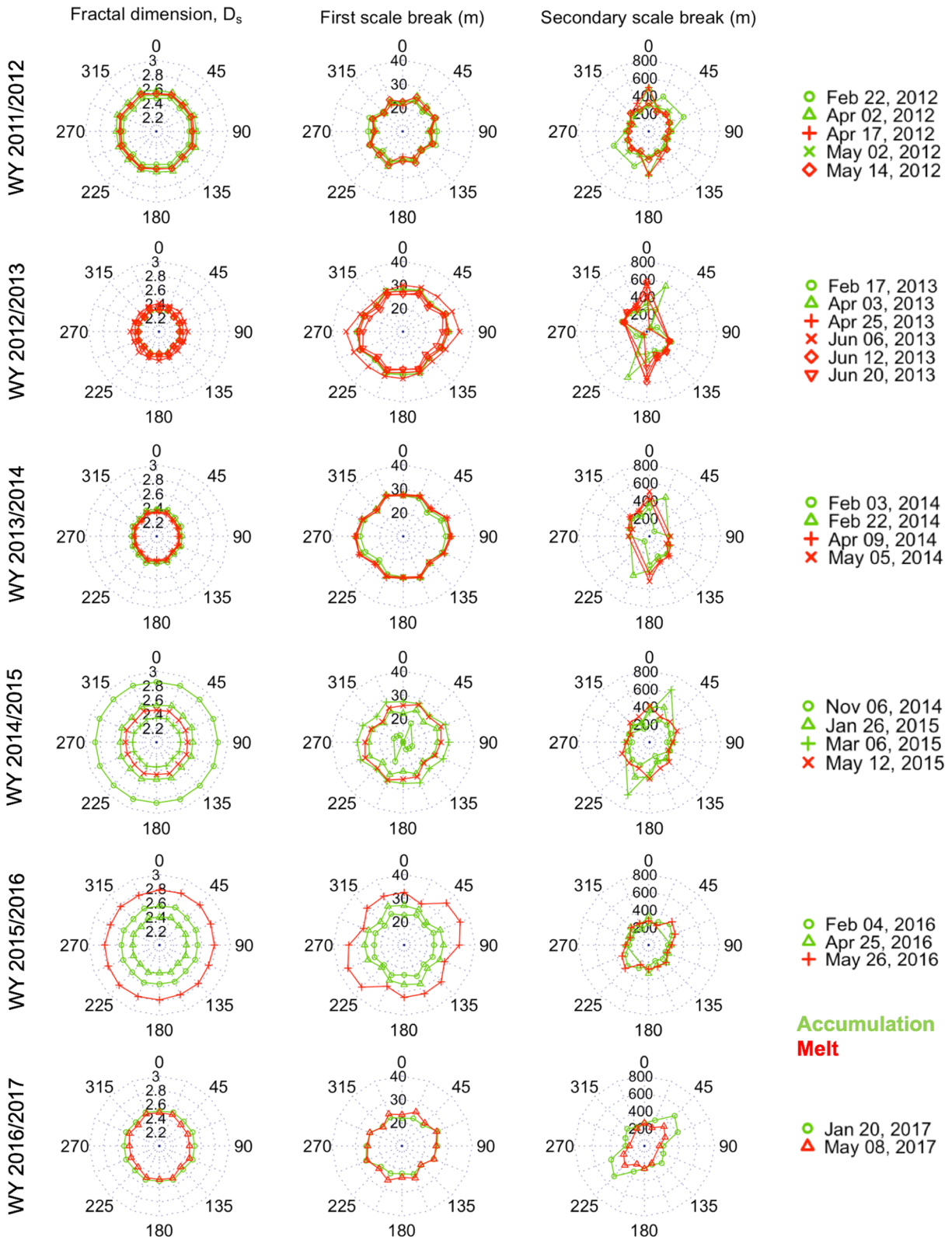
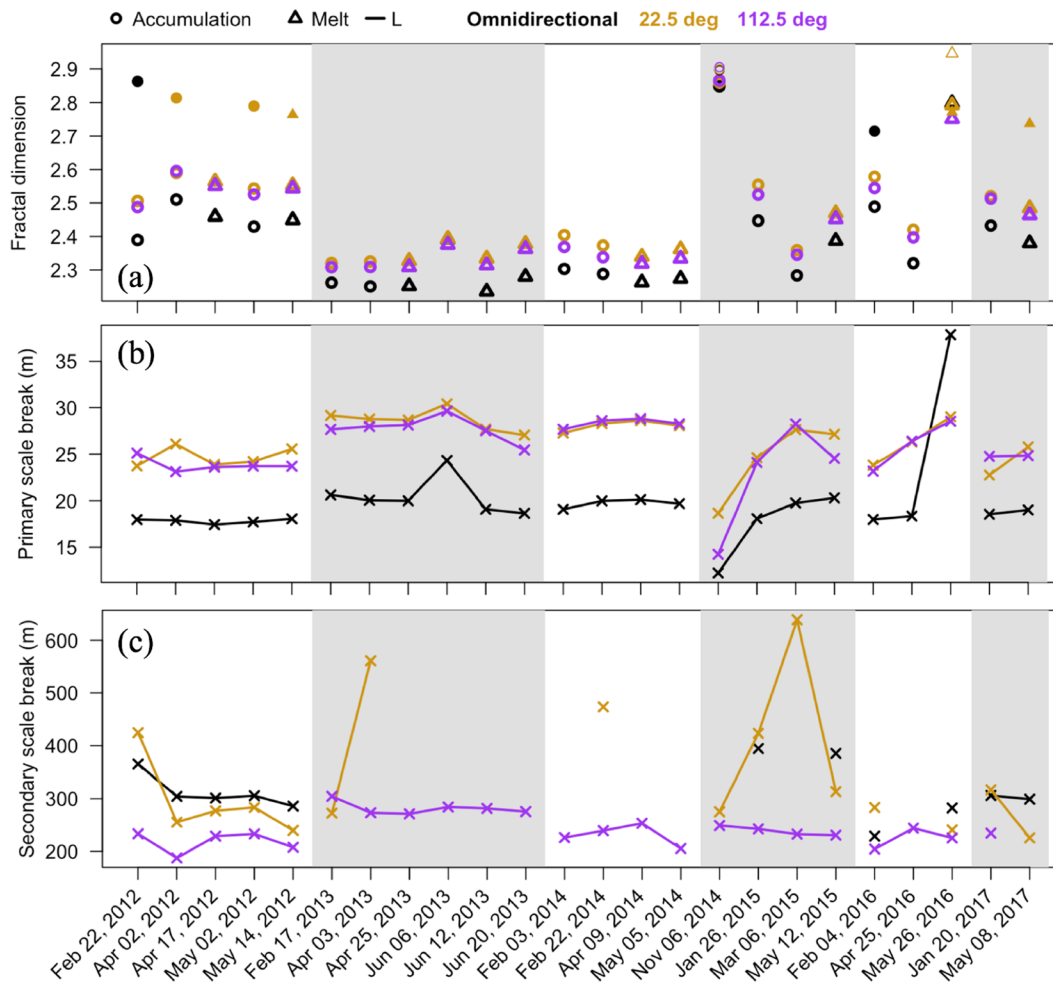**Figure 6.** Snow depth fractal parameters by azimuth, grouped per snow season.

Figure 7. Temporal evolution of snow depth fractal parameters through different snow seasons (white and shaded areas), derived from omnidirectional (black), 22.5° (gold) and 112.5° (purple) snow depth variograms: (a) short-range fractal dimension, (b) primary (short-range) scale break, and (c) secondary (long-range) scale break. Open thick and filled symbols are used to distinguish between short- and long-range fractal dimensions, respectively, and open thin symbols represent medium-range fractal dimensions.

3.3. Controls on Snow Depth Scaling Patterns

In this section, we analyze possible explanations for the scaling behavior of snow depth. Figure 8 displays omnidirectional and directional variograms for snow-free topography, together with fractal dimensions by azimuth. The results in Figure 8a demonstrate that terrain has a fractal distribution up to a scale break of 216 m and slightly less in the case of directional variograms (Figure 8b). Such breaks—although smaller —have the same order of magnitude than the secondary, long-range scale breaks found for snow depth distributions (e.g., Figure 7). Moreover, the directional distribution of D for snow-free topography (Figure 8c) is similar to the directionality of snow depth scale breaks (L_1) for the last melt season scans (Figure 4b), suggesting that the anisotropic behavior of shallow snow cover is caused by terrain influences. A direct comparison between scale break anisotropies for snow depth and snow-free topography cannot be made since scale breaks for the latter variable are only detected for a few directions (Figure 8b).

Figure 9 displays boxplots with short-range fractal dimensions and scale break lengths—derived from omnidirectional and directional (22.5° and 112.5°) variograms—stratified by type of scan (accumulation vs. melt; Figures 9a and 9c) and type of snow season (high-snow vs. low-snow seasons; Figures 9b and 9d). These results illustrate that the amount of snow accumulation appears to have the largest impact on the snow depth scaling patterns. With the exception of L_1 perpendicular to prevailing winds (22.5°), the snowpack development period (accumulation vs. melt) does not appear to explain variations in fractal parameters,
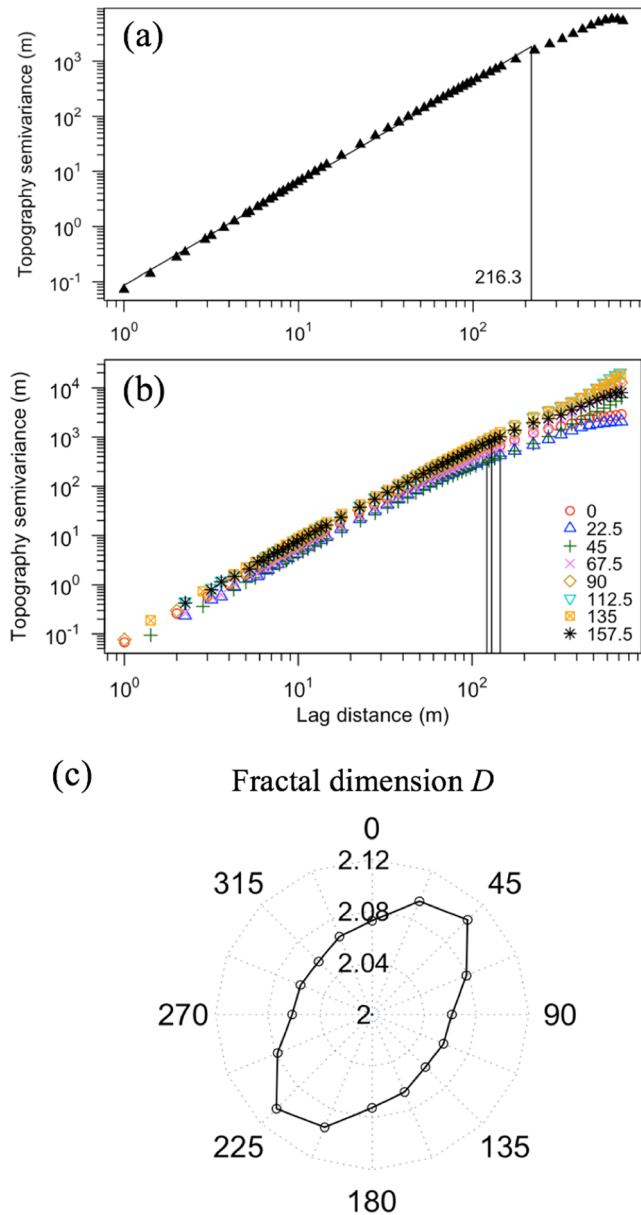
Figure 8. (a) Omnidirectional and (b) directional variograms for bare-earth topography, where vertical lines represent scale break lengths, and diagonal lines represent log–log linear models with $R^2 > 0.9$. (c) Short-range fractal dimension by azimuth.

whereas the type of season (low vs. high snow) provides significant differences (i.e., low p values) in most cases. Specifically, short-range fractal dimensions—either directional or omnidirectional—are always larger during low-snow seasons, reflecting larger spatial variability in snow depth, and larger scale breaks are detected during high-snow seasons.

The above results encourage us to explore simple metrics that can be used to infer the scaling pattern of snow depth over a specific domain. Figure 10 examines possible dependencies between fractal parameters and basin-wide snow descriptors, including domain averaged snow depth (mean SD), coefficient of variation (CV), and snow-covered area (SCA). Specifically, we analyze omnidirectional and directional short-range fractal dimension (D_S) and scale break length (L_1), finding the strongest relationships for fractal parameters perpendicular to dominant winds. Significant, negative Spearman rank correlations are obtained between D_S and domain-averaged snow depth, with the strongest relationships along 112.5° ($\rho = -0.84$). The results indicate that the spatial pattern of snow depth becomes smoother as more snow accumulates in the catchment. Conversely, we obtain positive correlations between D_S and CV, with $\rho \sim 0.46$–0.54. Such a result may be intuitive since the fractal dimension is interpreted here as a measure of surface irregularity, and higher CV values correspond to greater variation in snow depth over short distances.

Mean SD also provides predictive power on L_1 ($\rho \sim 0.62$–0.76), indicating that the scale range over which accumulation process relationships are consistent is greater under high-snow conditions. In general, weaker relationships are obtained between the fractal parameters examined here and SCA (right panels in Figure 10), which is likely due to the fact that SCA is relatively insensitive to total mean snow depth over much of the range of conditions studied. Finally, we found no significant correlations between the magnitude of anisotropies—quantified as difference between maximum and minimum directional fractal parameters from each lidar scan—and basin-averaged snow depth descriptors (Figure S3).

4. Discussion

The temporal extension of lidar-derived data sets used here allows a stronger demonstration of temporal consistency in snow depth scaling patterns—especially near maximum accumulation—in comparison to previous studies (Clemenzi et al., 2018; Deems et al., 2008; Helfricht et al., 2014; Schirmer & Lehning, 2011). All snow depth maps reveal a very strong spatial correlation (with $R^2 \geq 0.99$) up to a scale break on the order of tens of meters, followed by differing sp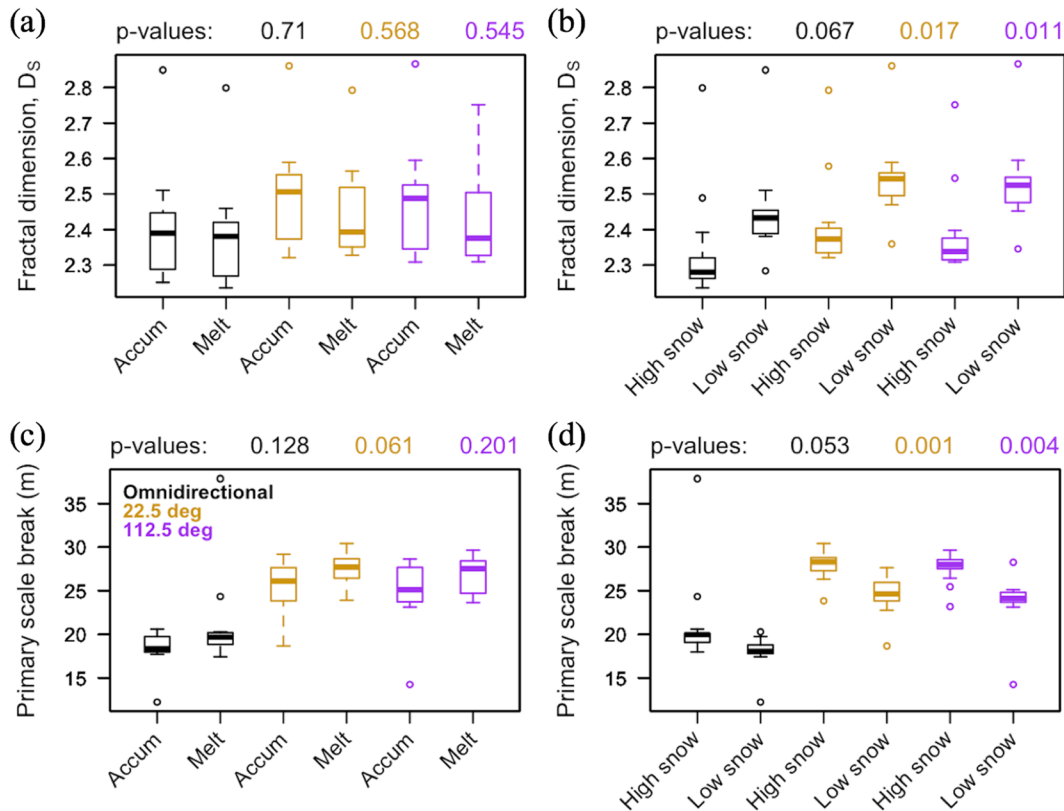atial structures. A novel aspect of this study is the second scale break aligned with prevailing winds (292.5°)—which can be followed by fractal behavior.

In addition to contributing to a fundamental understanding of snow depth patterns, which could be combined with advances in snow density measurement and modeling to estimate SWE, the temporal stability in scaling behavior across snow seasons has practical implications for guidance on modeling decisions. For example, the results from fractal analysis can be used to address the challenge of informing snow model scale decisions and whether processes like snow redistribution should be explicitly represented (Blöschl, 1999; Clark et al., 2011). Past studies agree that detailed attention is needed on the interplay between meteorological variables (i.e., local wind speed and direction) and scale breaks in snow depth, snow-free topography, and vegetation (e.g., Clemenzi et al., 2018; Deems et al., 2006). Trujillo et al. (2007) recommended that model scales shorter than the scale break in snow depth are needed to explicitly

Figure 9. Comparison of snow depth fractal parameter values obtained from: (a, c) accumulation ($n = 13$) vs. melt season ($n = 11$) lidar scans; and (b, d) high-snow ($n = 11$) vs. low-snow ($n = 13$) seasons. The reported *p* values result from applying *t* tests to contrast fractal parameter samples from omnidirectional (black), 22.5° (gold), and 112.5° (purple) variograms.

simulate interactions with local winds, surface concavities, trees, and rocks. To that end, we suggest that model resolutions below 15 m should be adopted for the Izas experimental catchment based on the scale break lengths obtained—either from omnidirectional and directional variograms. Nevertheless, the results may still be sensitive to wind field calculations (e.g., Mott & Lehning, 2010; Musselman et al., 2015) or the type of spatial discretization (e.g., Clark et al., 2011; Marsh et al., 2018). Along these lines, the lack of spatial correlation between the first and the secondary scale break lengths suggests that snow processes in this domain could be represented with a single unit, that is, a grouped response unit (GRU) or a hydrologic response units (HRU) whose characteristic scale lies within those limits (i.e., 40–150 m). The effects of these and other geospatial decisions on snow model simulations at the hillslope or catchment scales will be examined in future investigations.

Variogram analysis may also help to design predictor variables in statistical models for snow depth. Revuelto, López-Moreno, Azorin-Molina, & Vicente-Serrano et al. (2014) incorporated wind effects to model the spatial distribution of snow depth at the Izas experimental catchment through the maximum upwind slope parameter (S_x; Winstral & Marks, 2002). They used lidar data sets from a low-snow season (2011/2012) and a high-snow season (2012/2013), finding that the inclusion of S_x in regression models at a 200-m search distance and 315° (NW) or 270° (W) directions contributed to better predictions of snow depth. The search distance and directions are similar to the secondary scale break lengths (185–300 m) detected here along 112.5° (Figure 7)—that is, parallel to dominant wind directions (Figure 2). Moreover, the similarity between the short-range omnidirectional scale break lengths (Figure 7) and the optimal search distance (25 m) found by Revuelto, López-Moreno, Azorin-Molina, & Vicente-Serrano et al. (2014) for the TPI parameter supports the potential of TPI as a temporally consistent predictor for snow depth. More generally, these results suggest that the choice of TPI and S_x search distances should be informed by omnidirectional and directional variogram analyses, respectively, rather than by a trial and error process.
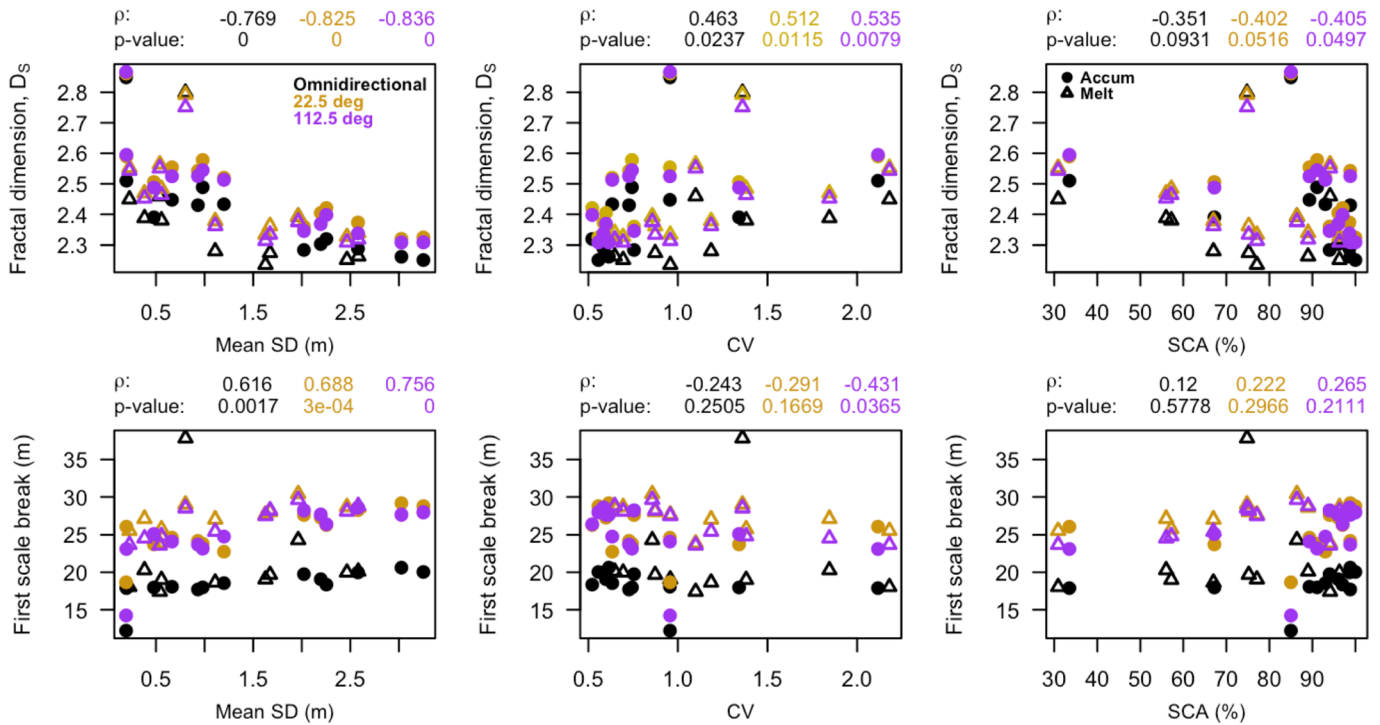
Figure 10. Scatter plots with omnidirectional and directional (22.5° azimuth—perpendicular to dominant wind direction—and 112.5° azimuth—aligned with dominant wind direction) snow depth fractal parameters vs. snow depth descriptive statistics for the entire domain. The strength of the relationship is quantified by Spearman rank correlation coefficients and *p* values.

An interesting result is the catchment-scale temporal consistency of omnidirectional scale break lengths for snow depth (Figure 7c). With the exception of snow distributions on 6 November 2014 and 26 May 2016— shallow outlier scan dates—omnidirectional values are near 20 m, which are remarkably similar to scale breaks reported in other sites worldwide. Helfricht et al. (2014) obtained scale breaks on the order of 20 m over ice-free terrain in a glacierized area in Austria. Clemenzi et al. (2018) found scale breaks of 20–22 m for snow depth on a glacier in Switzerland. Nevertheless, it should be noted that the magnitude of these breaks varies with specific site characteristics (e.g., presence and type of vegetation, bare ground, or ice topography) and their interaction with meteorological variables (Trujillo et al., 2007). For example, Schirmer and Lehning (2011) analyzed the snow depth distribution at an alpine (nonvegetated) site in Switzerland, finding different scale breaks in wind-protected (6 m) vs. wind-exposed (20 m) slopes and large variations in scale break lengths during the same snow season. Further work is needed to document and understand the physical mechanisms that determine the existence and magnitude of scale breaks across diverse global mountain environments.

The results presented in Figure 10 suggest that fractal analysis could be used to create initial conditions for snow model simulations with a statistical approach (e.g., a hierarchical Bayesian model) based on (i) a model to predict basin-wide snow depth statistics from climate forecasts and (ii) a model to predict fractal parameters using snow depth statistics. Given the nonlinear relationships found here, one could explore generalized linear models (McCullagh & Nelder, 1989), local regression methods (Loader, 1999), or machine learning techniques (e.g., Broxton et al., 2019; Snauffer et al., 2018). Ultimately, predicted fractal parameters could be used to generate an ensemble of random snow cover fields (e.g., Shook & Gray, 1997) to represent uncertainty in initial hydrologic conditions for snowmelt simulations.

It should be noted that our results are derived for a single catchment and—although consistent with many previous studies—are impacted by specific climatic and physiographic characteristics. Other limitations include the use of only one weather station since the wind measurements used here are not necessarily representative for the entire domain and the smaller number of lidar data sets available for the last few snow seasons. Finally, the variogram analysis used to estimate fractal parameters may introduce uncertainties

arising from possible overestimations (underestimations) of small (large) fractal dimensions (Wen & Sinding-Larsen, 1997). Although spatial and temporal fractal patterns are ubiquitous in nature—in particular, hydroclimatic variables—certain ambiguities around their formal detection and characterization exist, especially in limited-data geophysical applications (e.g., Cox & Wang, 1993; Fleming, 2014; Khaliq et al., 2009; Sun et al., 2006). Therefore, the development of theoretical methods and practical algorithms for robust detection of fractal behavior is a pertinent topic for future investigations.

5. Conclusions

We have examined temporal variations in snow depth scaling patterns using 24 TLS measurements of snow depth in relation to terrain topography and meteorological observations in a subalpine catchment. Fractal parameters were obtained from omnidirectional and directional variograms computed for 1-m resolution TLS snow depth maps acquired during six snow seasons (2011–2017). Our results corroborate previous findings on the short-range fractal behavior of snow depth up to a scale break of the order of tens of meters and the interannual consistency of these scaling characteristics, as reported in other regions worldwide (Clemenzi et al., 2018; Deems et al., 2008; Helfricht et al., 2014; Schirmer & Lehning, 2011). However, for most dates, there is no evidence of fractal structure beyond this break, as documented in previous studies at other sites (e.g., Clemenzi et al., 2018; Deems et al., 2006; Schirmer & Lehning, 2011). A striking result is a persistent long-range scale break of the order of 185–300 m, which is aligned with the dominant wind direction. Other conclusions are as follows:

1. Omnidirectional scale break lengths in snow depth show similar magnitude to the optimal search distance found by Revuelto, López-Moreno, Azorin-Molina, & Vicente-Serrano (2014) for the TPI—a topographic predictor for snow depth at the Izas experimental catchment.
2. Long-range (secondary) scale breaks in snow depth aligned with prevailing winds are of the same order of magnitude as the optimal search distance (200 m) found by Revuelto, López-Moreno, Azorin-Molina, & Vicente-Serrano (2014) for the upwind slope parameter S_x.
3. No clear links are found between directional variations in snow depth fractal dimension (D_S) and prevailing winds, reasserting that such relationship will depend on the particular landscape characteristics (e.g., vegetation, terrain exposure, and glacier topography) and their interaction with wind fields (Clemenzi et al., 2018).
4. Scale break anisotropies (L_1) in shallow snow cover during snowmelt periods can be explained by bare-earth terrain scaling patterns.
5. Based on the fractal analysis results, model scales ~15 m are recommended for this catchment to best represent interactions of snow with local topographic features and wind in distributed models. Additionally, snow processes between the first and secondary scale breaks (approximately 40–150 m) could be represented by a single HRU or GRU whose characteristic scale lies within those limits.

The results presented here suggest that variogram analysis is likely to provide useful information for designing explanatory variables (predictors) that can be used in statistical models that predict snow depth. Moreover, scale breaks in snow depth may be helpful to inform the spatial configuration of physically based snow models. Ongoing efforts are oriented to assess the effects of related decisions—in particular, the delineation of HRUs—on the accuracy of a distributed blowing snow model under historical and future climate conditions.

References

Alipour, M. H., Rezakhani, A. T., & Shamsai, A. (2016). Seasonal fractal-scaling of floods in two U.S. water resources regions. *Journal of Hydrology*, *540*, 232–239. https://doi.org/10.1016/j.jhydrol.2016.06.016

Anderton, S. P., White, S. M., & Alvera, B. (2004). Evaluation of spatial variability in snow water equivalent for a high mountain catchment. *Hydrological Processes*, *18*(3), 435–453. https://doi.org/10.1002/hyp.1319

Andreadis, K. M., Storck, P., & Lettenmaier, D. P. (2009). Modeling snow accumulation and ablation processes in forested environments. *Water Resources Research*, *45*, W05429. https://doi.org/10.1029/2008WR007042

Arnold, N. S., & Rees, W. G. (2003). Self-similarity in glacier surface characteristics. *Journal of Glaciology*, *49*(167), 547–554. https://doi.org/10.3189/172756503781830368

Barnett, T. P., Adam, J. C., & Lettenmaier, D. P. (2005). Potential impacts of a warming climate on water availability in snow-dominated regions. *Nature*, *438*(7066), 303–309. https://doi.org/10.1038/nature04141

Blöschl, G. (1999). Scaling issues in snow hydrology. *Hydrological Processes*, *13*(14–15), 2149–2175. https://doi.org/10.1002/(SICI)1099-1085(199910)13:14/15%3C2149::AID-HYP847%3E3.0.CO;2-8

Broxton, P. D., van Leeuwen, W. J. D., & Biederman, J. A. (2019). Improving snow water equivalent maps with machine learning of snow survey and lidar measurements. *Water Resources Research*, *55*, 3739–3757. https://doi.org/10.1029/2018WR024146

Clark, M. P., Hendrikx, J., Slater, A. G., Kavetski, D., Anderson, B., Cullen, N. J., et al. (2011). Representing spatial variability of snow water equivalent in hydrologic and land-surface models: A review. *Water Resources Research*, *47*, W07539. https://doi.org/10.1029/2011WR010745

Clemenzi, I., Pellicciotti, F., & Burlando, P. (2018). Snow depth structure, fractal behavior, and interannual consistency over Haut Glacier d'Arolla, Switzerland. *Water Resources Research*, *54*, 7929–7945. https://doi.org/10.1029/2017WR021606

Cox, B. L., & Wang, J. S. Y. (1993). Fractal surfaces: Measurement and applications in the earth sciences. *Fractals*, *01*(01), 87–115. https://doi.org/10.1142/s0218348x93000125

Deems, J. S., Fassnacht, S. R., & Elder, K. J. (2006). Fractal distribution of snow depth from lidar data. *Journal of Hydrometeorology*, *7*(2), 285–297. https://doi.org/10.1175/JHM487.1

Deems, J. S., Fassnacht, S. R., & Elder, K. J. (2008). Interannual consistency in fractal snow depth patterns at two Colorado mountain sites. *Journal of Hydrometeorology*, *9*(5), 977–988. https://doi.org/10.1175/2008JHM901.1

Deems, J. S., Painter, T. H., & Finnegan, D. C. (2013). Lidar measurement of snow depth: A review. *Journal of Glaciology*, *59*(215), 467–479. https://doi.org/10.3189/2013JoG12J154

Fassnacht, S. R., & Deems, J. S. (2006). Measurement sampling and scaling for deep montane snow depth data. *Hydrological Processes*, *20*(4), 829–838. https://doi.org/10.1002/hyp.6119

Fleming, S. W. (2014). A non-uniqueness problem in the identification of power-law spectral scaling for hydroclimatic time series. *Hydrological Sciences Journal*, *59*(1), 73–84. https://doi.org/10.1080/02626667.2013.851384

Freudiger, D., Kohn, I., Seibert, J., Stahl, K., & Weiler, M. (2017). Snow redistribution for the hydrological modeling of alpine catchments. *Wiley Interdisciplinary Reviews Water*, *4*(5), e1232. https://doi.org/10.1002/wat2.1232

He, S., Ohara, N., & Miller, S. N. (2019). Understanding subgrid variability of snow depth at 1-km scale using lidar measurements. *Hydrological Processes*, *33*(11), 1525–1537. https://doi.org/10.1002/hyp.13415

Helfricht, K., Schöber, J., Schneider, K., Sailer, R., & Kuhn, M. (2014). Interannual persistence of the seasonal snow cover in a glacierized catchment. *Journal of Glaciology*, *60*(223), 889–904. https://doi.org/10.3189/2014JoG13J197

Hurst, H. (1951). Long-term storage capacity of reservoirs. *Transactions of the American Society of Civil Engineers*, *116*(1), 770–799.

James, N. A., & Matteson, D. S. (2014). ecp: An R package for nonparametric multiple change point analysis of multivariate data the ecp package. *Journal of Statistical Software*, *62*(7), 1–16.

Khaliq, M. N., Ouarda, T. B. M. J., & Gachon, P. (2009). Identification of temporal trends in annual and seasonal low flows occurring in Canadian rivers: The effect of short- and long-term persistence. *Journal of Hydrology*, *369*(1–2), 183–197. https://doi.org/10.1016/j.jhydrol.2009.02.045

Kirchner, J. W., Feng, X., & Neal, C. (2000). Fractal stream chemistry and its implications for contaminant transport in catchments. *Nature*, *403*(6769), 524–527. Retrieved from. https://doi.org/10.1038/35000537

Korres, W., Reichenau, T. G., Fiener, P., Koyama, C. N., Bogena, H. R., Cornelissen, T., et al. (2015). Spatio-temporal soil moisture patterns–A meta-analysis using plot to catchment scale data. *Journal of Hydrology*, *520*, 326–341. https://doi.org/10.1016/j.jhydrol.2014.11.042

Kuchment, L. S., & Gelfan, A. N. (2001). Statistical self-similarity of spatial variations of snow cover: Verification of the hypothesis and application in the snowmelt runoff generation models. *Hydrological Processes*, *15*(18), 3343–3355. https://doi.org/10.1002/hyp.1032

Lehning, M., Grünewald, T., & Schirmer, M. (2011). Mountain snow distribution governed by an altitudinal gradient and terrain roughness. *Geophysical Research Letters*, *38*, L19504. https://doi.org/10.1029/2011GL048927

Li, L., & Pomeroy, J. W. (1997). Estimates of threshold wind speeds for snow transport using meteorological data. *Journal of Applied Meteorology*, *36*(3), 205–213. https://doi.org/10.1175/1520-0450(1997)036%3C0205:EOTWSF%3E2.0.CO;2

Loader, C. (1999). *Local regression and likelihood*. New York: Springer.

López-Moreno, J. I., Fassnacht, S. R., Heath, J. T., Musselman, K. N., Revuelto, J., Latron, J., et al. (2013). Small scale spatial variability of snow density and depth over complex alpine terrain: Implications for estimating snow water equivalent. *Advances in Water Resources*, *55*, 40–52. https://doi.org/10.1016/j.advwatres.2012.08.010

López-Moreno, J. I., Gascoin, S., Herrero, J., Sproles, E. A., Pons, M., Alonso-González, E., et al. (2017). Different sensitivities of snowpacks to warming in Mediterranean climate mountain areas. *Environmental Research Letters*, *12*(7), 74,006. https://doi.org/10.1088/1748-9326/aa70cb

López-Moreno, J. I., Pomeroy, J. W., Revuelto, J., & Vicente-Serrano, S. M. (2013). Response of snow processes to climate change: Spatial variability in a small basin in the Spanish Pyrenees. *Hydrological Processes*, *27*(18), 2637–2650. https://doi.org/10.1002/hyp.9408

Mandelbrot, B. (1977). *Fractals: Form, chance and dimension*. (W.H. Freeman, Ed.). San Francisco.

Mandelbrot, B. (1982). *The fractal geometry of nature*. (W. Freeman, Ed.). San Francisco.

Mandelbrot, B. B. (1988). An introduction to multifractal distribution functions. In *Random fluctuations and pattern growth: Experiments and models*, (pp. 279–291). Dordrecht: Springer. https://doi.org/10.1007/978-94-009-2653-0_40

Mandelbrot, B. B., & Wallis, J. R. (1968). Noah, Joseph, and operational hydrology. *Water Resources Research*, *4*(5), 909–918. https://doi.org/10.1029/WR004i005p00909

Mankin, J. S., Viviroli, D., Singh, D., Hoekstra, A. Y., & Diffenbaugh, N. S. (2015). The potential for snow to supply human water demand in the present and future. *Environmental Research Letters*, *10*(11), 114016. https://doi.org/10.1088/1748-9326/10/11/114016

Mark, D. M., & Aronson, P. B. (1984). Scale-dependent fractal dimensions of topographic surfaces: An empirical investigation, with applications in geomorphology and computer mapping. *Mathematical Geology*, *16*(7), 671–683. https://doi.org/10.1007/BF01033029

Marsh, C. B., Spiteri, R. J., Pomeroy, J. W., & Wheater, H. S. (2018). Multi-objective unstructured triangular mesh generation for use in hydrological and land surface models. *Computers and Geosciences*, *119*(April), 49–67. https://doi.org/10.1016/j.cageo.2018.06.009

Matteson, D. S., & James, N. A. (2014). A nonparametric approach for multiple change point analysis of multivariate data. *Journal of the American Statistical Association*, *109*(505), 334–345. https://doi.org/10.1080/01621459.2013.849605

McCullagh, J., & Nelder, P. (1989). *Generalized linear models (second edition)*. London: Chapman and Hall/CRC. https://doi.org/10.1007/978-1-4899-3242-6

Mendoza, P. A., Musselman, K. N., Revuelto, J., Deems, J. S., López-Moreno, J. I., & McPhee, J. (2020). Snow depth fractal behavior at the Izas experimental catchment from 2011 to 2017 [Data set]. https://doi.org/10.5281/zenodo.3661414

Mendoza, P. A., Rajagopalan, B., Clark, M. P., Cortés, G., & McPhee, J. (2014). A robust multimodel framework for ensemble seasonal hydroclimatic forecasts. *Water Resources Research*, *50*, 6030–6052. https://doi.org/10.1002/2014WR015426

Molz, F. J., Rajaram, H., & Lu, S. (2004). Stochastic fractal-based models of heterogeneity in subsurface hydrology: Origins, applications, limitations, and future research questions. *Reviews of Geophysics*, *42*, RG1002. https://doi.org/10.1029/2003RG000126

Mott, R., & Lehning, M. (2010). Meteorological modeling of very high-resolution wind fields and snow deposition for mountains. *Journal of Hydrometeorology*, *11*(4), 934–949. https://doi.org/10.1175/2010JHM1216.1

Mott, R., Schirmer, M., & Lehning, M. (2011). Scaling properties of wind and snow depth distribution in an Alpine catchment. *Journal of Geophysical Research*, *116*, D06106. https://doi.org/10.1029/2010JD014886

Musselman, K. N., Pomeroy, J. W., Essery, R. L. H., & Leroux, N. (2015). Impact of windflow calculations on simulations of alpine snow accumulation, redistribution and ablation. *Hydrological Processes*, *29*(18), 3983–3999. https://doi.org/10.1002/hyp.10595

Oliver, M., & Webster, R. (2007). *Geostatistics for environmental scientists*. New York: John Wiley & Sons.

Olsson, J., Niemczynowicz, J., & Berndtsson, R. (1993). Fractal analysis of high-resolution rainfall time series. *Journal of Geophysical Research*, *98*(D12), 23265. https://doi.org/10.1029/93JD02658

Perkins, T. R., Pagano, T. C., & Garen, D. C. (2009). Innovative operational seasonal water supply forecasting technologies. *Journal of Soil and Water Conservation*, *64*(1), 15A–17A. https://doi.org/10.2489/jswc.64.1.15A

Revuelto, J., Azorin-Molina, C., Alonso-González, E., Sanmiguel-Vallelado, A., Navarro-Serrano, F., Rico, I., & López-Moreno, J. I. (2017a). Meteorological and snow distribution data in the Izas experimental catchment (Spanish Pyrenees) from 2011 to 2017. *Earth System Science Data*, *9*(2), 993–1005. https://doi.org/10.5194/essd-9-993-2017

Revuelto, J., Azorin-Molina, C., Alonso-González, E., Sanmiguel-Vallelado, A., Navarro-Serrano, F., Rico, I., & López-Moreno, J. I. (2017b). Observations of snowpack distribution and meteorological variables at the Izas Experimental Catchment (Spanish Pyrenees) from 2011 to 2017 [Data set]. https://doi.org/10.5281/zenodo.848277

Revuelto, J., López-Moreno, J. I., Azorin-Molina, C., & Vicente-Serrano, S. M. (2014). Topographic control of snowpack distribution in a small catchment in the central Spanish Pyrenees: Intra- and inter-annual persistence. *The Cryosphere*, *8*(5), 1989–2006. https://doi.org/10.5194/tc-8-1989-2014

Revuelto, J., López-Moreno, J. I., Azorin-Molina, C., Zabalza, J., Arguedas, G., & Vicente-Serrano, S. M. (2014). Mapping the annual evolution of snow depth in a small catchment in the Pyrenees using the long-range terrestrial laser scanning. *Journal of Maps*, *10*(3), 379–393. https://doi.org/10.1080/17445647.2013.869268

Rosenberg, E. A., Wood, A. W., & Steinemann, A. C. (2011). Statistical applications of physically based hydrologic models to seasonal streamflow forecasts. *Water Resources Research*, *47*, W00H14. https://doi.org/10.1029/2010WR010101

Schirmer, M., & Lehning, M. (2011). Persistence in intra-annual snow depth distribution: 2. Fractal analysis of snow depth development. *Water Resources Research*, *47*, W09517. https://doi.org/10.1029/2010WR009429

Scipiõn, D. E., Mott, R., Lehning, M., Schneebeli, M., & Berne, A. (2013). Seasonal small-scale spatial variability in alpine snowfall and snow accumulation. *Water Resources Research*, *49*, 1446–1457. https://doi.org/10.1002/wrcr.20135

Shook, K., & Gray, D. (1996). Small-scale spatial structure of spatial snowcovers. *Hydrological Processes*, *10*(10), 1283–1292. https://doi.org/10.1002/(SICI)1099-1085(199610)10:10%3C1283::AID-HYP460%3E3.0.CO;2-M

Shook, K., & Gray, D. M. (1997). Synthesizing shallow seasonal snow covers. *Water Resources Research*, *33*(3), 419–426. https://doi.org/10.1029/96WR03532

Skøien, J. O., Blöschl, G., & Western, A. W. (2003). Characteristic space scales and timescales in hydrology. *Water Resources Research*, *39*(10), 1223. https://doi.org/10.1029/2002WR001736

Snauffer, A. M., Hsieh, W. W., Cannon, A. J., & Schnorbus, M. A. (2018). Improving gridded snow water equivalent products in British Columbia, Canada: Multi-source data fusion by neural network models. *The Cryosphere*, *12*(3), 891–905. https://doi.org/10.5194/tc-12-891-2018

Sun, W., Xu, G., Gong, P., & Liang, S. (2006). Fractal analysis of remotely sensed images: A review of methods and applications. *International Journal of Remote Sensing*, *27*(22), 4963–4990. https://doi.org/10.1080/01431160600676695

Tarboton, D. G., Bras, R. L., & Rodriguez-iturbe, I. (1988). The fractal nature of river networks. *Water Resources Research*, *24*(8), 1317–1322.

Tedesche, M. E., Fassnacht, S. R., & Meiman, P. J. (2017). Scales of snow depth variability in high elevation rangeland sagebrush. *Frontiers of Earth Science*, *11*(3), 469–481. https://doi.org/10.1007/s11707-017-0662-z

Trujillo, E., Ramírez, J. A., & Elder, K. J. (2007). Topographic, meteorologic, and canopy controls on the scaling characteristics of the spatial distribution of snow depth fields. *Water Resources Research*, *43*, W07409. https://doi.org/10.1029/2006WR005317

Trujillo, E., Ramírez, J. A., & Elder, K. J. (2009). Scaling properties and spatial organization of snow depth fields in sub-alpine forest and alpine tundra. *Hydrological Processes*, *23*(11), 1575–1590. https://doi.org/10.1002/hyp.7270

Viviroli, D., Archer, D. R., Buytaert, W., Fowler, H. J., Greenwood, G. B., Hamlet, A. F., et al. (2011). Climate change and mountain water resources: Overview and recommendations for research, management and policy. *Hydrology and Earth System Sciences*, *15*(2), 471–504. https://doi.org/10.5194/hess-15-471-2011

Viviroli, D., Dürr, H. H., Messerli, B., Meybeck, M., & Weingartner, R. (2007). Mountains of the world, water towers for humanity: Typology, mapping, and global significance. *Water Resources Research*, *43*, W07447. https://doi.org/10.1029/2006WR005653

Wen, R., & Sinding-Larsen, R. (1997). Uncertainty in fractal dimension estimated from power spectra and variograms. *Mathematical Geology*, *29*(6), 727–753. https://doi.org/10.1007/BF02768900

Winstral, A., & Marks, D. (2002). Simulating wind fields and snow redistribution using terrain-based parameters to model snow accumulation and melt over a semi-arid mountain catchment. *Hydrological Processes*, *16*(18), 3585–3603. https://doi.org/10.1002/hyp.1238